# Theoretical Study of 1,4-Dioxane in Aqueous Solution and Its Experimental Interaction with Nano-$CuSO_4$

***Ali, Lailla I.; Abdel Halim, Shimaa A.****[+]

*Department of Chemistry, Faculty of Education, Ain Shams University, Roxy 11711, Cairo, EGYPT*

***Gomaa, Esam A.****[+]

*Department of Chemistry, Faculty of Science, Mansoura University, Mansoura, EGYPT*

***Sanad, Sameh G.***

*Department of Chemistry, Faculty of Education, Ain Shams University, Roxy 11711, Cairo, EGYPT*

**ABSTRACT:** *The electronic structure, Non-Linear Optical (NLO) properties and Natural Bonding Orbital (NBO) analysis of 1,4-dioxane were investigated using the theoretical study of Density Functional Theory (DFT) calculations at the B3LYP/6-311G (d,p) level of theory. The optimized structure is nonlinear as indicated from the dihedral angles. Natural bonding orbital analysis has been analyzed in terms of the hybridization of each atom, natural charges (Core, Valence and Rydberg), bonding and antibonding orbital's second order perturbation energy ($E^{(2)}$). The calculated $E_{HOMO}$ and $E_{LUMO}$ energies of the title molecule can be used to explain the charge transfer in the molecule and to calculate the global properties; the chemical hardness ($\eta$), softness (S) and electronegativity ($\chi$). The NLO parameters: static dipole moment ($\mu$), polarizability ($\alpha$), anisotropy polarizability ($\Delta\alpha$) and first order hyperpolarizability ($\beta_{tot}$) of the studied molecule have been calculated at the same level of theory. The Molecular Electrostatic Potential (MEP) and Electro Static Potential (ESP) for 1,4-dioxane were investigated and analyzed. Also, the electronic absorption spectra were discussed by Time-Dependent Density Functional Theory (TD-DFT) calculations for 1,4-dioxane in 10% ethanol/water. From the experimental conductance measurements, the association thermodynamic parameters ($K_A$, $\Delta G_A$, $\Delta H_A$ and $\Delta S_A$) and complex formation thermodynamic parameters ($K_f$, $\Delta G_f$, $\Delta H_f$ and $\Delta S_f$) of nano-$CuSO_4$ in the presence of 1,4-dioxane as a ligand in 10% ethanol-water at different temperatures (298.15, 303.15, 308.15 and 313.15 $^oK$) were applied and calculated.*

**KEYWORDS** *DFT/TD-DFT; NLO and NBO analysis; Association parameters; Formation parameters; nano-$CuSO_4$; 1,4-dioxane.*

## INTRODUCTION

Juaristi and coworkers, [1] studied the anomeric effect in several 1,3 dioxane derivatives and concluded that in compounds with a good substitute for hydrogen bonding, an axial conformer is preferred. In mono-substituted

***** *To whom correspondence should be addressed.*

*+ E-mail: shimaaquantum@ymail.com ; eahgomaa65@yahoo.com*

*1021-9986/2019/3/43-60 18/$/6.08*

cyclohexanes with OH and OM, the equatorial conformer is preferred as an explanation reproduced by ab initio calculations. The preference for the equatorial conformer is even greater for the Me substituent and all these behaviors fit well with the results of calculations [2]. The marked preference of the equatorial orientation of the Methyl substitute has been attributed fundamentally to hyperconjugative interactions and not to steric effects and the same conclusion has been reached for cyclohexanol [3,4]. Recently, *Dabbagh* and *Coworkers*, [5] studied the structure, conformation of 1,4-dioxane, configuration of the imine group of the imidoyl moiety and the anomeric effect of cyclohexanes using X-ray crystallographic analysis. 1,4-Dioxanes have been studied extensively [6], and it was determined that their structures were comparable to certain antibiotics such as valinomycin [7], enniatin B, and nonactin, [8]. These structural similarities led to the use of 1,4-dioxanes as reference models to study the binding and delivery mechanisms of these antibiotics to their targeted biological sites [9]. This implicit solvation model approach is popular because it allows the calculation of the properties of a molecule in solution without prohibitively expensive computational cost. The NLO properties depend on the extent of Charge Transfer (CT) interaction across the conjugative paths and the electron transfer ability of an aromatic ring and on its ionization potential (IP) and electron affinity (EA) [10, 11]. Linear polarizability $\langle \Delta\alpha \rangle$ and first order hyperpolarizability $\langle \beta \rangle$ are required for the rational design of optimized materials for photonic devices such as electro-optic modulators and all-optical switches [12, 13]. Natural Bond Orbital (NBO) analysis was originated as a technique for studying hybridization and covalence effects in polyatomic wave functions. The work of *Foster* and *Winhold* [14] was extended by *Reed et al.,* [15] who employed NBO analysis to molecules that exhibited particularly H-bonded and other strongly bound van der Waals complexes. The filled NBOs $\sigma$ of the "natural Lewis structure" is well adapted to describing covalence effects in molecules [15]. However, the general transformation to NBOs also leads to orbitals that are unoccupied in the formal Lewis structure and that may be used to describe noncovalent effects. the symbols $\sigma$ and $\sigma^*$ are used in a generic sense to refer to filled and unfilled orbitals of the formal Lewis structure, though the former orbitals may actually be core orbitals (*CR*), lone pairs (*LP*), σ or $\pi$ bonds ($\sigma$, $\pi$), and so forth, and the latter may be $\sigma$ or $\pi$ antibonds ($\sigma^*$, $\pi^*$), extravalence shell Rydberg (*RY**) orbital's. The object of our studies is to shed more light on the geometric structures (bond lengths, bond angles, and dihedral angles) and ground state properties of 1,4-Dioxanes. To achieve this goal, we have used Density Functional Theory (DFT-B3LYP) and basis set 6-311G (d,p), Natural Bonding Orbital's (NBO) and Non Linear Optical (NLO) analysis to identify and characterize the forces that govern the structure of the title molecule. The results from natural bonding orbital analysis have been valuated in terms of the hybridization of each atom, natural charges (Core, Valence, and Rydberg), bonding and antibonding orbital's second order perturbation energy ($E^{(2)}$), exact configurations and Lewis and non-Lewis electrons. In addition to investigating the effect of solvent polarity on the observed spectra and hence, predicting the relative stabilities, extent of charge transfer character and assignment of the observed electronic transitions bands as localized, delocalized and/or of Charge Transfer (CT) have been facilitated by Density Functional Theory (DFT) and Time-Dependent Density Functional Theory (TD-DFT) calculations. The electronic structure of molecules usually manifests itself in the electronic absorption and emission spectra. This manifestation enables the detailed understanding of the forces that govern the electronic structure of the studied compound 1,4-Dioxane.

Copper sulfate is a fungicide material. Some fungi are able to elevate levels of copper ions. Algae can be controlled with small concentrations of copper sulfate. Copper sulfate inhibits the growth of bacteria. It can also cause cell death through apoptosis and necrosis [16, 17].

## EXPERIMENTAL SECTION

### *Preparation of materials*

The nano-$CuSO_4$ solution in water ($1.0 \times 10^{-3}$ M, 5 mL) and the solution of 1,4-Dioxane in 10% ethanol/water ($1.0 \times 10^{-4}$ M, 100 ml) were placed in the titration cell, thermostated at the preset temperature and the conductance of the solution was measured after the solution reached thermal equilibrium. Then, a known amount of mixed solvents (what solvent? Please be specific) was added in a stepwise manner using a calibrated micropipette. The conductance of the solution was measured after each addition until the desired

constant reading was achieved. The specific conductance values were recorded using a conductivity bridge JENCO – 3173 COND. with a cell constant equal to 1. The temperature was adjusted at 298.15, 303.15, 308.15 and 313.15K [18, 19].

***Computational method***

Calculations have been performed using Khon-Sham′s Density Functional Theory (DFT) method subjected to the gradient-corrected hybrid density functional B3LYP method [20]. This function is a combination of the Becke′s three parameters non-local exchange potential with the non-local correlation functional of *Lee et al.* [21]. For each structure, a full geometry optimization was performed using this function [21] and the 6-311G (p,d) basis set [22] as implemented by Gaussian 09 package [23]. All geometries were visualized either using GaussView 5.0.9 [24] or chemcraft 1.6 software packages. No symmetry constraints were applied during geometry optimization. Also, the total static dipole moment ($\mu$), $\langle\Delta\alpha\rangle$, $\langle\beta\rangle$ values were calculated by using the following equations [25- 27]:

$$\mu = \left(\mu_x^2 + \mu_y^2 + \mu_z^2\right)^{1/2} \quad (1)$$

$$< a >= \frac{1}{3}\left(a_{xx} + a_{yy} + a_{zz}\right)$$

$$\Delta a = \left(\left(a_{xx} - a_{yy}\right)^2 + \left(a_{yy} - a_{zz}\right)^2 + \left(a_{zz} - a_{xx}\right)^2 / 2\right)^{1/2}$$

$$< \beta >= \left(\beta_x^2 + \beta_y^2 + \beta_z^2\right)^{1/2}$$

Where

$$\beta_x = \beta_{xxx} + \beta_{xyy} + \beta_{xzz} \quad (2)$$

$$\beta_y = \beta_{yyy} + \beta_{xyy} + \beta_{xzz}$$

$$\beta_z = \beta_{zzz} + \beta_{xxz} + \beta_{yyz}$$

By using HOMO and LUMO energy values for a molecule, electronegativity, and chemical hardness can be calculated as follows: $\chi = (I + A)/2$ (electronegativity), $\eta = (I - A)/2$ (chemical hardness), $S = 1/2\eta$ (chemical softness) where $I$ and $A$ are ionization potential and electron affinity, and $I = -E_{HOMO}$ and $A = -E_{LUMO}$, respectively [28, 29]. The population analysis has also been performed by the natural bond orbital method [30] at B3LYP/6-311G (d,p) level of theory using natural bond orbital (NBO) under Gaussian 09 program package. The second-order Fock matrix was used to evaluate the donor-acceptor interactions in the NBO basis [31]. The interactions result in a loss of occupancy from the localized NBO of the idealized Lewis structure into an empty non-Lewis orbital. For each donor ($i$) and acceptor ($j$), the stabilization energy $E^{(2)}$ associated with the delocalization $i \rightarrow j$ is estimated as

$$E^{(2)} = \Delta E_{ij} = q_i \left(F(ij)^2 / \varepsilon_j - \varepsilon_i'\right) \quad (3)$$

Where $q_i$ is the donor orbital occupancy, $\varepsilon_i$, and $\varepsilon_j$ are diagonal elements and $F(ij)$ is the off-diagonal NBO Fock matrix element. The conversion factors for $\alpha$, $\beta$, $\gamma$, and HOMO and LUMO energies in atomic and cgs units: 1 atomic unit (a.u.) = $0.1482 \times 10^{-24}$ electrostatic unit (esu) for polarizability; 1 a.u. = $8.6393 \times 10^{-33}$ esu for first hyperpolarizability; 1 a.u. = 27.2116 eV (electron volt) for HOMO and LUMO energies.

## RESULTS AND DISCUSSION

***Association thermodynamic parameters.***

The association constants for nano-$CuSO_4$ in the presence of the ligand 1,4-Dioxane in ethanol and water at different temperatures (298.15, 303.15, 308.15 and 313.15 K) were calculated by using equation (4) [32-37].

$$K_A = \Lambda 0\left(\Lambda_0 - S(Z)\Lambda_m\right) \quad (4)$$

$$C_m \Lambda_m^2 S(Z)^{2\gamma\pm 2}$$

Where $\Lambda_m$, $\Lambda_0$ are the molar and limiting molar conductance of nano-$CuSO_4$ in the presence of the ligand respectively, $C_m$ is the molar concentration of nano-$CuSO_4$, S(Z) is Fouss – Shedlovsky factor, equal with unity for strong electrolytes, $\gamma_\pm$ is the mean activity coefficient.

The association constants at different temperatures (298.15, 303.15, 308.15 and 313.15 $^oK$) for nano-$CuSO_4$ in the presence of 1,4-dioxane are estimated and listed in Table 1. The estimated values indicate that the association constants increase as the temperature increases.

The relationship between the molar conductance ($\Lambda_m$) of $CuSO_4$ in the presence of the ligand and the square root of concentration ($C^{1/2}$) for nano-$CuSO_4$ in the presence of 1,4-dioxane at different temperatures

***Table 1: Association constants of 1,4-dioxane (in 10% ethanol-90% water) at different temperatures.***

| T (°K) | C | $C^{1/2}$ | $\Lambda_m$ | $\Lambda_0$ | Log $\gamma_\pm$ | $\gamma_\pm$ | $K_A$ |
|---|---|---|---|---|---|---|---|
| 298.15 | $9.091 \times 10^{-5}$ | 0.0095 | 399.296 | 1800 | -0.0048 | 0.977 | 182233.5 |
| 303.15 | $9.091 \times 10^{-5}$ | 0.0095 | 458.6 | 1800 | -0.0048 | 0.977 | 132300.6 |
| 308.15 | $9.091 \times 10^{-5}$ | 0.0095 | 721.5 | 1390 | -0.0048 | 0.977 | 20570.4 |
| 313.15 | $9.091 \times 10^{-5}$ | 0.0095 | 546.695 | 1200 | -0.0048 | 0.977 | 30227.78 |

***Table 2: Association constants, free energies, enthalpies and entropies of Association of 1,4-dioxane (in 10% ethanol-90% water).***

| T (K) | $\Delta G_A$ | $\Delta H_A$ | $T\Delta S$ | $\Delta S_A$ |
|---|---|---|---|---|
| 298.15 | -30.0325 | -309.54 | -279.508 | -0.9374 |
| 303.15 | -29.7289 | -309.54 | -279.811 | -0.0092 |
| 308.15 | -25.4498 | -309.54 | -284.09 | -0.9219 |
| 313.15 | -26.865 | -309.54 | -282.675 | -0.9027 |

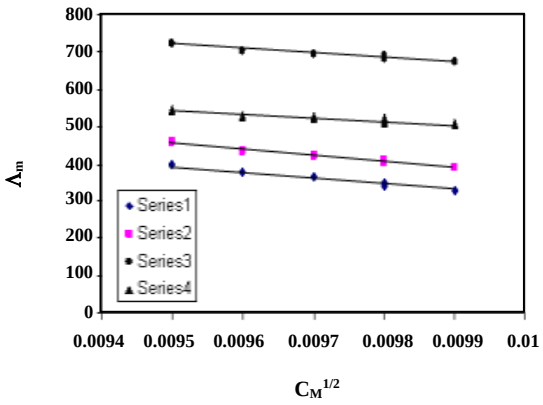


***Fig. 1: The relationship between $\Lambda_m$ and $C^{1/2}$ for nano-$CuSO_4$ in the presence of 1,4-dioxane (in 10% ethanol-90% water).***

is illustrated in Fig. 1. The data show an inverse relationship between the molar conductance and ($C^{1/2}$). Also, the molar conductance increases with increasing the temperature.

The calculated free energies, enthalpies and entropies of association for nano-$CuSO_4$ in the presence of 1,4-dioxane at (298.15, 303.15, 308.15 and 313.15 K) are listed in Table 2. The data show that free energies of association decrease in negativity with increasing the temperature. Negative free energies at all temperatures indicate the spontaneous character of the reaction.

The calculated values for the formation constants, free energies, enthalpies and entropies of formation for nano-$CuSO_4$ in the presence of 1,4-dioxane at (298.15, 303.15, 308.15 and 313.15 K) are listed in Table 3. The data in Table 3 show that the formation of constants and free energies in case of (1:1) metal to ligand are more favorable than (1:2) metal to ligand. This may be explained because the free energies in case of (1:1) metal to ligand are more negative than (1:2) metal to ligand. The calculated free energies of formation values in Table 3 have decreased as the temperature increases, meaning that a lower temperature favors the complex formation.

The relationship between log $K_A$ and 1/T in the presence of 1,4-dioxane for nano-$CuSO_4$ is shown in Fig. 2.

***Formation thermodynamic parameters***

The relationship between the molar conductance ($\Lambda_m$) and the molar ratio of Metal to Ligand (M/L) indicate the formation of 1:2 and 1:1 stoichiometric complexes. The formation constants ($K_f$) for the 1:2 and 1:1 (M:L) complexes were calculated by using equation (5) [38-41].

$$K_f = \frac{\Lambda_m - \Lambda_{obs}}{(\Lambda_{obs} - \Lambda_{ML})[L]} \quad (5)$$

Where $\Lambda_M$ is the limiting molar conductance of the salt alone, $\Lambda_{obs}$ is the molar conductance of solution during titration, [L] is the concentration of ligand and $\Lambda_{ML}$ is the molar conductance of the complex. By drawing the relationship between the molar conductance ($\Lambda_m$) and the molar ratio of metal to ligand concentrations ($C_M/C_L$), the resulting figures confirm the formation of 1:2 and 1:1 stoichiometric complexes. The relationship between $\Lambda_m$ and $C_M/C_L$ at (298.15, 303.15, 308.15 and

***Table 3: Formation constants, free energies, enthalpies and entropies of formation of dioxane (in 10% ethanol-90% water).***

| TEMP | M:L | $K_f$ | $\Delta G_f$ | $\Delta H_f$ | $\Delta S_f$ |
|---|---|---|---|---|---|
| 298.15 | 1:2 | 9860.189 | -22.8007 | -79.6218 | -0.1906 |
| | 1:1 | 128025.9 | -29.1571 | -123.5868 | -0.3167 |
| 303.15 | 1:2 | 7101.32 | -22.3557 | -79.6218 | -0.1889 |
| | 1:1 | 87745.81 | -28.6937 | -123.5868 | -0.3130 |
| 308.15 | 1:2 | 4399.646 | -21.4976 | -79.6218 | -0.1886 |
| | 1:1 | 41734.68 | -27.8503 | -123.5868 | -0.3107 |
| 313.15 | 1:2 | 4716.742 | -22.0276 | -79.6218 | -0.1839 |
| | 1:1 | 45180.88 | -27.9117 | -123.5868 | -0.3055 |

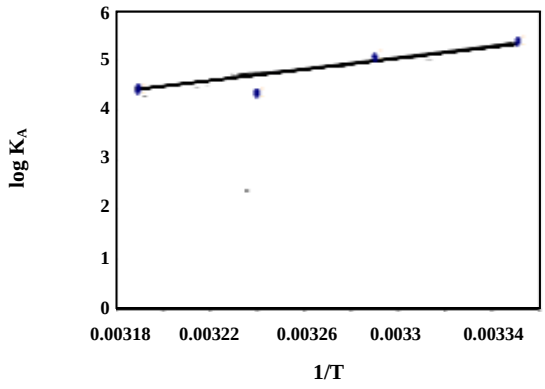


***Fig. 2: The relationship between log $K_A$ and 1/T for nano-$CuSO_4$ in the presence of 1,4-dioxane (in 10% ethanol-90% water).***

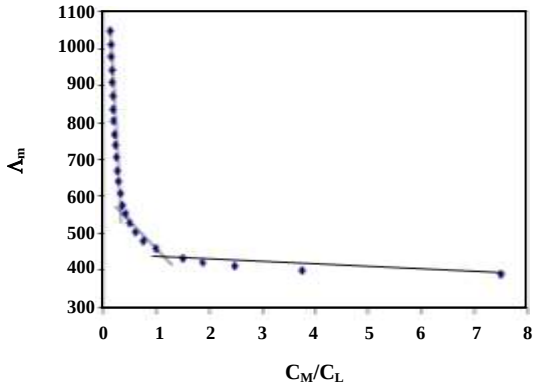


***Fig. 4: The relation between $\Lambda_m$ and $C_M/C_L$ at 303.15 °K for nano-$CuSO_4$ in the presence of 1,4-dioxane (in 10% ethanol-90% water).***

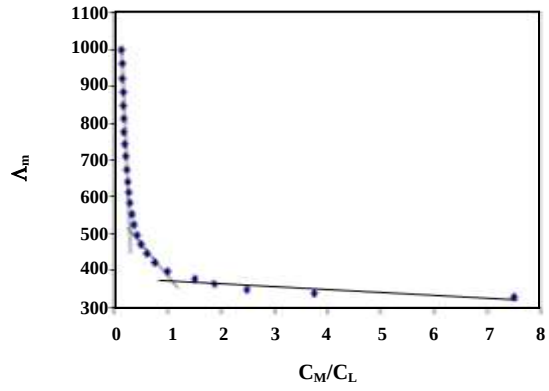


***Fig. 3: The relationship between $\Lambda_m$ and $C_M/C_L$ at 298.15 K for nano-$CuSO_4$ in the presence of 1,4-dioxane (in 10% ethanol-90% water).***

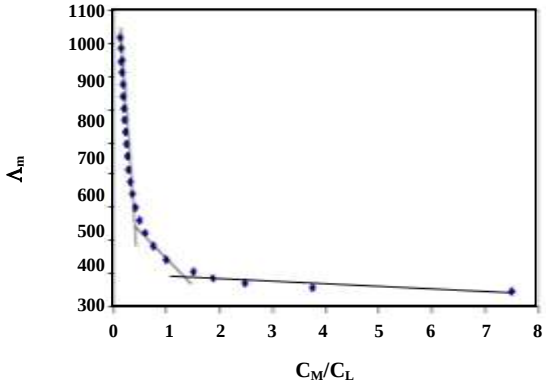


***Fig. 5: The relationship between $\Lambda_m$ and $C_M/C_L$ at 308.15 K for nano-$CuSO_4$ in the presence of 1,4-dioxane (in 10% ethanol-90% water).***

313.15 °K) for nano-$CuSO_4$ in the presence of 1,4-dioxane in ethanol/water mixed solvents are shown in Figs.3, 4, 5 and 6. Figs. 7 and 8 illustrate the relationship between log $K_f$ and 1/T when metal to ligand ratio is 1:2 and 1:1 respectively for nano-$CuSO_4$ in presence of 1,4-dioxane.

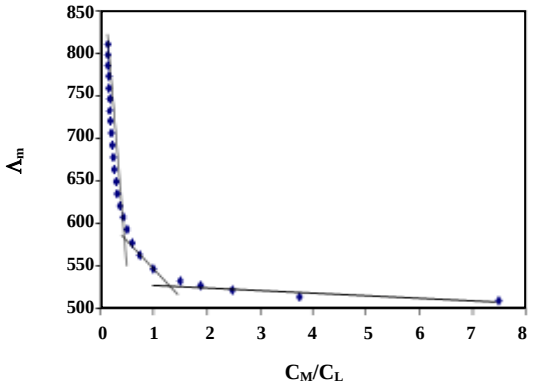


***Fig. 6: The relationship between $\Lambda_m$ and $C_M/C_L$ at 313.15 K for nano-$CuSO_4$ in the presence of 1,4-dioxane (in 10% ethanol-90% water).***

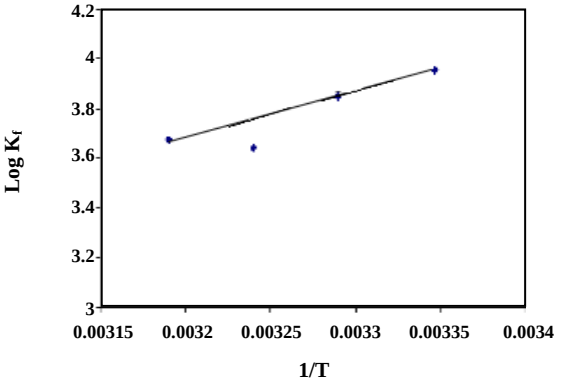


***Fig. 7: The relationship between log $K_f$ and 1/T when M:L is 1:2 for nano-$CuSO_4$ in the presence of 1,4-dioxane (in 10% ethanol-90% water).***

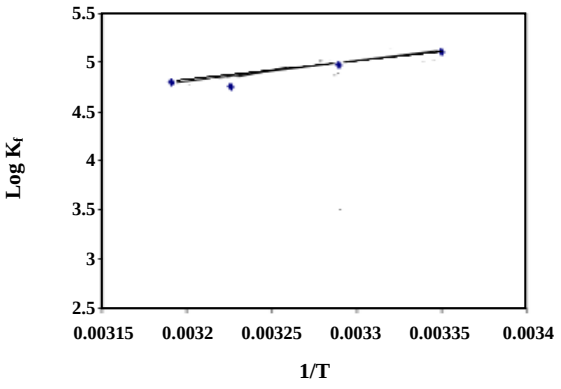


***Fig. 8: The relationship between log $K_f$ and 1/T when M:L is 1:1 for nano-$CuSO_4$ in the presence of 1,4-dioxane (in 10% ethanol-90% water).***

Fig. 9 TEM for nano-$CuSO_4$ (a-d). All images in Fig. 9 (a-d) were measured by using JEOL HRTEM - JEM 2100 (JAPAN). The figures show that the TEM of $CuSO_4$ obtained in ethanol are irregular spheres in the form of cylinders. The diameter is in the range of 10-77.86 nm. The small sizes in the range between 10, 12.05 to 20.76 nm are collected to give bigger sizes to 77.86 nm (a-c). These different sizes were proved also by x-ray diffraction which gave crystal sizes in the same order (d). The non-homogeneity in the sizes of nano-$CuSO_4$ particles need be controlled during the primary preparation of the samples.

***Ground state properties***

The total energy ($E_T$), the energy of the highest occupied molecular orbital ($E_{HOMO}$), energy of the lowest unoccupied molecular orbital ($E_{LUMO}$), energy gap ($E_g$) and dipole moment (μ) of 1,4-dioxane are presented in Table 4. The optimized structure of the title molecule is obtained using the B3LYB/6-311G (p,d) level, numbering system, net charge, vector of dipole moment and the charge density maps of HOMO and LUMO are presented in Fig. 10. From Table 4 and Fig. 10 one can reveal the following:

- The ionization energy (I.E) of 1,4-dioxane which measures its donating property (oxidation power) is 5.22 eV (c.f. Table 4).
- The electron affinity (E.A) which measures the accepting property (reducing power) is 0.28 eV.
- The calculated energy gaps, (Eg), which measure the chemical activity of free 1,4-dioxane is 4.95 eV (≈ 114.1 kcal).
- The theoretically computed dipole moment (μ), which measures the polarity or charge separation over the title molecule is 0.00 D.

***Geometric Structure***

The optimized geometric parameters (bond lengths, bond angles, and dihedral angles) of 1,4-dioxane using B3LYP/6-311G (d,p) level of theory are listed in Table 5 and are compared with the available x-ray experimental data [42]. The observed bond lengths of $C_1$-$C_2$, $C_1$-$O_{10}$, and $C_1$-$H_5$ in 1,4-dioxane are 1.479 Å, 1.380 Å, and 1.030 Å respectively, while the obtained theoretical values are 1.327 Å, 1.388 Å, and 1.079 Å respectively [42]. The computed bond angles of $<C_1O_{10}C_2$, $<O_{10}C_4H_8$, $<C_2C_3O_9$,

***Table 4: Total energy, the energy of HOMO and LUMO, energy gap and dipole moment of 1,4-Dioxane computed at the B3LYP/6-311G (d,P) level of theory.***

| Compounds | $E_T$ (au) | $E_{HOMO}$ (eV) | $E_{LUMO}$ (eV) | $E_{gap}$ (eV) | μ (Debye) |
|---|---|---|---|---|---|
| 1,4-Dioxane | -305.27849 | -5.22485 | -0.27826 | 4.946592 | 0 |

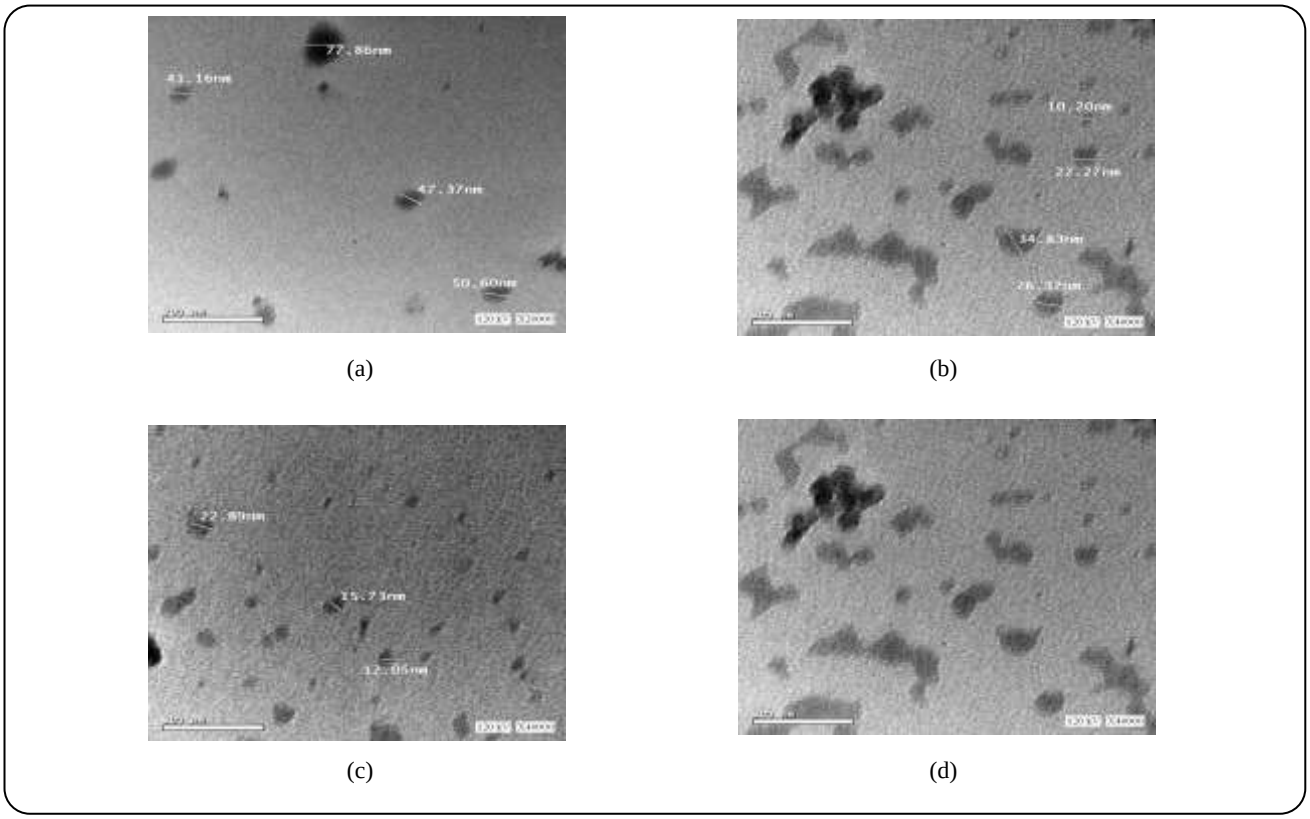


***Fig. 9: TEM for nano-$CuSO_4$ (a-d). The four images (a-d) were measured using JEOL HRTEM – JEM 2100 (JAPAN). The images show that TEM of CuSO4 obtained in ethanol are irregular spheres in the form of cylinders. The diameters are in the range of 10-77.86 nm. The small sizes in the range between 10, 12.05 to 20.76 nm are collected to give bigger sizes till 77.86 nm (a-c). These irregular sizes were proved also by x- ray diffraction measurement, which shows crystal sizes in the same order (d). The non homogeneity in sizes for nano copper sulfate particles need to be controlled during the primary preparation of the samples.***

and $<C_3C_4H_7$ are 123.95°, 112.79°, 112.11°, and 123.26° respectively, while the experimental values are 118.99°, 111.92°, 110.63°, and 116.87° respectively. In conclusion, the bond lengths and angles calculated by B3LYP methods are in good agreement with the experimental values. The Mullikan net charge observed on active centers O1 and O2 are -0.301 and -0.301 respectively. The most stable geometry of the studied compound is a planar structure as indicated from the dihedral angles (c.f. Table 5).

***Natural Bonding Orbital (NBO) Analysis***

The NBO analysis provides an efficient method for studying intra- and intermolecular bonding and interaction among bonds, and also enables a convenient basis for investigating charge transfer or conjugative interaction in molecular systems [43]. The larger the interacting stabilization energy $E^{(2)}$ value, the more intensive is the interaction between electron donors and the greater the extent of conjugation of the whole system. Delocalization of electron density between occupied Lewis type (bond or lone pair) NBO orbital's and formally unoccupied (antibonding or Rydberg) non Lewis NBO orbitals correspond to a stabling donor-acceptor interaction [44, 45]. NBO analysis was performed on the title molecule at the DFT/B3LYP/6-311G (d,p) level in order to elucidate the intramolecular rehybridization

***Table 5: Selected experimental and theoretical bond lengths, bond angles, dihedral angles and net charges for 1,4-Dioxane at the B3LYP/6-311G (d,P) level of theory.***

| Bond lengths (Å) | 1,4-Dioxane | X-ray [42] | Bond angle (°) | 1,4-Dioxane | X-ray [42] | Dihedral angles (°) | 1,4-Dioxane | X-ray [42] |
|---|---|---|---|---|---|---|---|---|
| $C_1 – C_2$ | 1.327 | 1.479 | $<C_2C_1O_{10}$ | 123. 946 | 118.987 | $C_2C_1H_5H_6$ | 0.0000 | 0.390 |
| $C_1 – H_5$ | 1.079 | 1.030 | $<C_3C_4H_7$ | 123.264 | 116.868 | $H_5C_1O_{10}C_4$ | 180.000 | 176.999 |
| $C1 – O_{10}$ | 1.388 | 1.380 | $<C_4O_{10}H_8$ | 112.790 | 111.925 | $C_3C_4O_9O_{10}$ | 0.0000 | 0.390 |
| | | | $<C_2C_3O_9$ | 112.108 | 110.635 | Net charges | | |
| | | | | | | $O_1$ | -0.301 | |
| | | | | | | $O_2$ | -0.301 | |

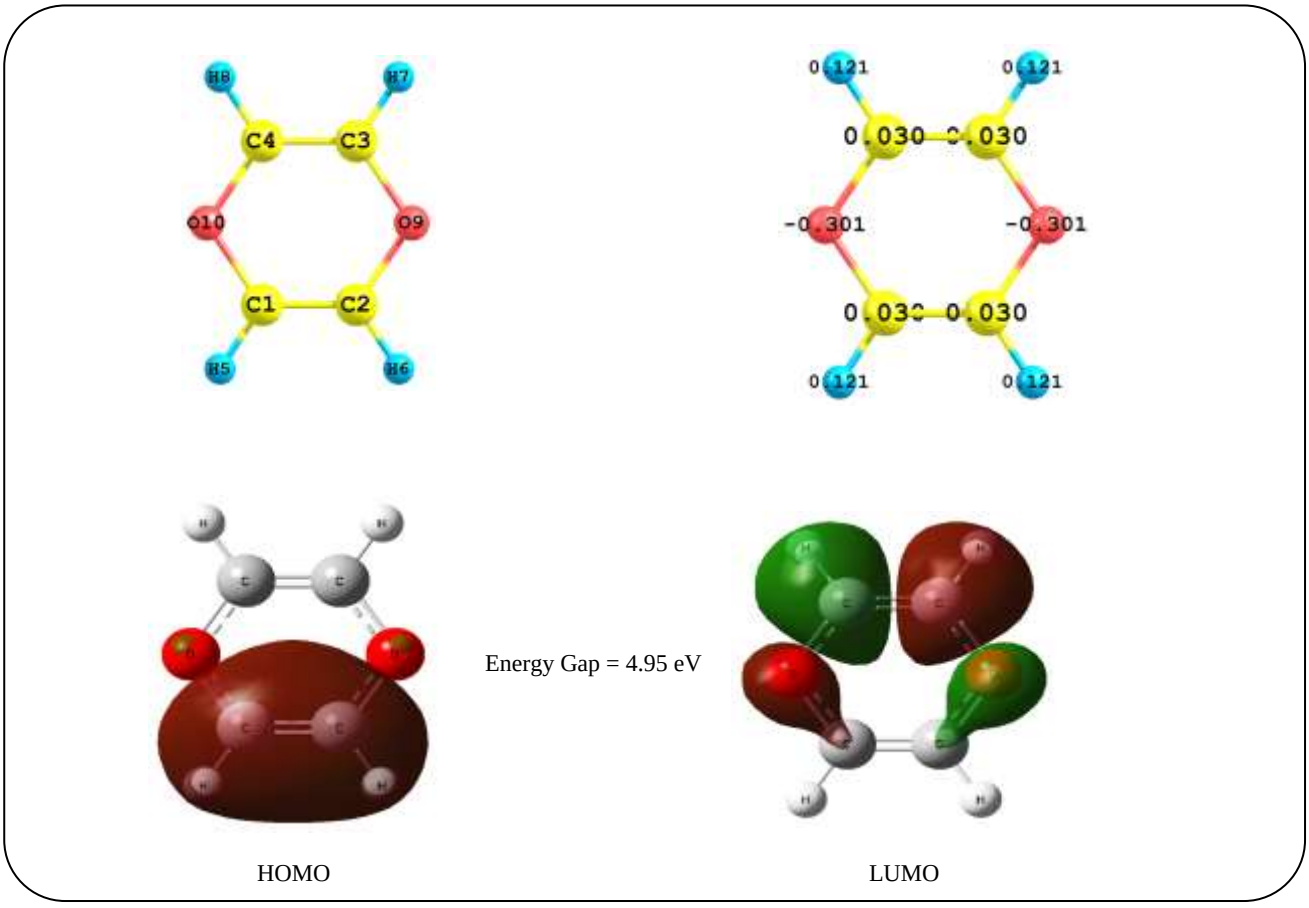


***Fig. 10: Optimized geometry, numbering system, net charge, HOMO and LUMO for 1,4-Dioxane using B3LYP/6-311G (d,p).***

and delocalization of electron density within the molecule. The molecular interaction is formed by the orbital overlap between σ (C-C) and σ∗(C-C) bond orbitals, which indicate that intramolecular charge (ICT) causes stabilization of the system. These interactions are observed as an increase in Electron Density (ED) in C-C antibonding orbital that weakens the respective bonds. The electron density of conjugated double as well as the single bonds of the conjugated ring (≈ 1.9e) clearly demonstrate strong delocalization inside the molecule [46].

*Donor-acceptor bonding in title molecules*

The perturbation energies of donor-acceptor interactions and the type of each bonding and antibonding orbitals,

***Table 6: Second Order Perturbation Theory Analysis of Fock Matrix in NBO Basis for 1,4-Dioxane by B3LYP/6-311G (d,p).***

| Donor 1,4-Dioxane | Type | ED(i)(e) | Acceptor | Type | ED(i)(e) | $E^{(2)a}$(kcal/mol) | E(j)-E(i)[b](a.u) | F(ij)[c](a.u) |
|---|---|---|---|---|---|---|---|---|
| BD C1-H5 | σ | 1.97559 | BD*C2-O9 | σ * | 0.02103 | 6.57 | 0.88 | 0.068 |
| BD C4-H8 | σ | 1.97559 | BD*C1-O10 | σ * | 0.02103 | 3.67 | 0.88 | 0.051 |
| LP(1) O10 | | 1.96299 | BD*C3-C4 | σ * | 0.01955 | 4.81 | 1.21 | 0.069 |
| LP(2) O9 | | 1.84559 | BD*C1-C2 | π * | 0.14743 | 26.59 | 0.35 | 0.086 |

*a) $E^{(2)}$ means energy of hyperconjugative interactions (stabilization energy). b) Energy difference between donor and acceptor i and j NBO orbitals. c) $F_{(i,j)}$ is the Fock matrix element between i and j NBO orbital. d)$LP_{(n)}$ is a valence lone pair orbital (n) on atom.*

***Table 7: Occupancy of natural orbitals (NBOs) and hybrids of 1,4-Dioxane by B3LYP/6-311G (d,p).***

| Donor Lewis-type (NBOs) 1,4-Dioxane | Occupancy | Hybrid | AO [%] |
|---|---|---|---|
| σ BD C1-H5 | 1.97559 | $sp^{2.11}$ | s(32.12%)p(67.83%)d(0.05%) |
| σ BD C4-H8 | 1.97559 | $sp^{2.11}$ | s(32.12%)p(67.83%)d(0.05%) |
| LP(1) O10 | 1.96299 | $sp^{1.39}$ | s(41.85%)p(58.12%)d(0.03%) |
| LP(2) O9 | 1.84559 | $p^{1.00}$ | s(0.00%)p(99.95%)d(0.05%) |

Fock-matrix element between donor and acceptor orbitals, occupancy of donor Lewis-type NBO's, hybridization and % AO of the studied molecule using B3LYP/6-311G (d,p) are presented in Tables 6 and 7. From Table 6 in our title molecule σ ($C_1$-$H_5$) → σ* ($C_2$-$O_9$) has 6.57 kJ/mol and LP (2) $O_9$ → π* ($C_1$-$C_2$) has 26.59 kJ/mol. Hence, they give stronger stabilization to the structure. From Table 7 it is noted that the maximum occupancies 1.97559, 1.96299 are obtained for σ ($C_1$-$H_5$), and LP (1) $O_{10}$, respectively. Therefore, these bonds are essentially controlled by the sp-character of the hybrid orbitals (c.f. Table 7).

*Natural Bonding Orbital (NBO) occupancy and hybrid orbitals*

The calculated natural hybrids on each atom and occupancies are given in Table 7. As seen from Table (7), the σ ($C_1$-$H_5$) bond is formed from $sp^{2,11}$ hybrids on carbon (which is a mixture of 32.12% *s*, 67.83% *p*, and 0.05% *d* atomic orbitals). On the other hand, LP (1) $O_{10}$ bond is formed from $sp^{1,39}$ hybrids on carbon (which is a mixture of 41.85% *s*, 58.12% *p*, and 0.03% *d* atomic orbital's). The LP (2) $O_9$ is formed from $p^{1.00}$ hybrid on carbon (which is a mixture of 0.00% *s*, 99.95% *p*, and 0.05% *d* atomic). The natural population analysis showed that 44 electrons in the free 1,4-dioxane are distributed on the sub shells as total Lewis (core and valence Lewis) and total non-Lewis (valence non-Lewis and Rydberg non-Lewis). The computed values and percentage of each are found below:

| | |
|---|---|
| Core | 11.99512 (99.959% of 12) |
| Valence Lewis | 31.45733 (98.304% of 32) |
| Total Lewis | 43.45245 (98.756% of 44) |
| Valence non-Lewis | 0.47922 (1.089% of 44) |
| Rydberg non-Lewis | 0.06833 (0.155% of 44) |
| Total non-Lewis | 0.54755 (1.244% of 44) |

*Natural charge and exact configuration*

The natural population analysis performed on the electronic structures of 1,4-dioxane clearly describes the distribution of electrons in various sub-shells of their atomic orbits. The accumulation of charges on the individual atom and the accumulation of electrons in the core, valence and Rydberg sub-shells and natural electronic configuration are also presented in Table 8. In our title molecule, the most electronegative center charge of -0.5249 and -0.5249 are accumulated on $O_9$, and $O_{10}$ atoms. According to an electrostatic point of view of the molecule, these electronegative atoms have tendencies to donate electrons. Also, it is found that the most electropositive center charges of 0.1937, 0.1937, 0.1937 and 0.1937 are accumulated on $H_5$, $H_6$, $H_7$, and $H_8$-atoms. According to an electrostatic point of view of the molecule, these electropositive atoms have tendencies to accept electrons. The natural electronic configuration of each electronegative and electropositive atom is listed in Table 8.

***Table 8: Natural Charge, Natural Population and Natural electronic Configuration of 1,4-Dioxane using B3LYP/6-311G(d,P).***

| Compound | Atom No. | Natural Charge | Natural Population | | | | Natural electronic Configuration |
|---|---|---|---|---|---|---|---|
| 1,4-Dioxane | | | Core | Valence | Rydberg | total | |
| | $C_1$ | 0.0687 | 1.999 | 3.9083 | 0.02406 | 5.93 | [core]2S(0.92)2p(2.99)3p(0.01)3d(0.01) |
| | $C_2$ | 0.0687 | 1.999 | 3.9083 | 0.02406 | 5.93 | [core]2S(0.92)2p(2.99)3p(0.01)3d(0.01) |
| | $C_3$ | 0.0687 | 1.999 | 3.9083 | 0.02406 | 5.93 | [core]2S(0.92)2p(2.99)3p(0.01)3d( 0.01) |
| | $C_4$ | 0.0687 | 1.999 | 3.9083 | 0.02406 | 5.93 | [core]2S(0.92)2p(2.99)3p(0.01)3d(0.01) |
| | $H_5$ | 0.1937 | 0 | 0.8044 | 0.00183 | 0.81 | 1S(0.80) |
| | $H_6$ | 0.1937 | 0 | 0.8044 | 0.00183 | 0.81 | 1S(0.80) |
| | $H_7$ | 0.1937 | 0 | 0.8044 | 0.00183 | 0.81 | 1S(0.80) |
| | $H_8$ | 0.1937 | 0 | 0.8044 | 0.00183 | 0.81 | 1S(0.80) |
| | $O_9$ | -0.5249 | 1.999 | 6.5139 | 0.01121 | 8.52 | [core]2S(1.61)2p(4.90)3p(0.01) |
| | $O_{10}$ | -0.5249 | 1.999 | 6.5139 | 0.01121 | 8.52 | [core]2S(1.61)2p(4.90)3p(0.01) |

*Core* *11.99512 (99.959% of 12)*
*Valence Lewis* *31.45733 (98.304% of 32)*
==========  ==========
*Total Lewis* *43.45245 (98.756% of 44)*
---
*Valence non-Lewis* *0.47922 (1.089% of 44)*
*Rydberg non-Lewis* *0.06833 (0.155% of 44)*
==========  ==========
*Total non-Lewis* *0.54755 (1.244% of 44)*

*Global reactivity descriptors*

The Frontier Molecular Orbital (FMO) energies of 1,4-dioxane were calculated using B3LYP/6-311G (d,p). The HOMO energy characterizes the electron giving ability, while the LUMO energy characterizes the electron withdrawing ability. The energy gap between HOMO and LUMO characterizes the molecular chemical stability and it is a critical parameter in determining molecular electrical transport properties because it is a measure of electron conductivity. From Fig. 11 and Table 9, HOMO energy is calculated as -5.225 eV and LUMO energy is calculated as -0.278 eV by using B3LYP/6-311G (d,p) level. The small energy gap between HOMO and LUMO indicates that charge transfer occurs within the title molecule and the molecule can be easily polarized. Using HOMO and LUMO energies, ionization potential and electron affinity can be explicated as $IP \approx -E_{HOMO,}$ $EA \approx -E_{LUMO.}$ The variation of electronegativity ($\chi$) values is supported by the electrostatic potential. For any two molecules, electrons will be partially transferred from one of low $\chi$ to that of high $\chi$ (electron flow from high chemical potential to low chemical potential). The chemical hardness ($\eta$) = ($IP - EA$)/2, electronegativity ($\chi$) = ($IP + EA$)/2, chemical potential (μ) = - ($IP + EA$)/2, and chemical softness ($S$) = 1/2$\eta$, values were calculated as 2.473, 2.751, -2.751 and 0.202 respectively. Obtained small $\eta$ value means that the charge transfer occurs in the molecule. Considering the $\eta$ values, a large HOMO - LUMO gap means a hard molecule and a small HOMO -LUMO gap means a soft molecule. Additionally, it can be said that the smaller HOMO – LUMO energy gap represents more reactive molecule.

*Other molecular properties*

The 3D plots of Highest Occupied Molecular Orbital (HOMO) and the Lowest Unoccupied Molecular Orbital (LUMO), Electrostatic Potential (ESP), Electron Density (ED), and the Molecular Electrostatic Potential (MEP) map for the title molecule at the B3LYP method with 6-311G (d,p) level are shown in Fig. 11. The ED plot for the title, a molecule shows a uniform distribution. While the negative ESP is more localized over the oxygen atoms, the positive ESP is localized on the rest of the molecule.

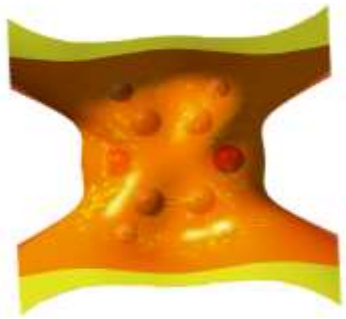

ESP

MEP

Total density

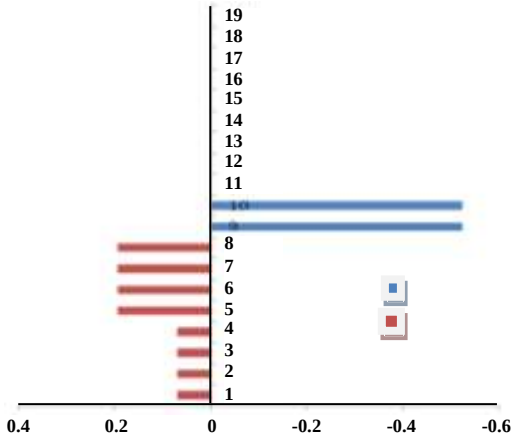


***Fig. 11: Molecular surfaces and atomic charge distribution (au) of the 1,4-Dioxane using B3LYP/6-311G (d,p).***

MEP has been used primarily for predicting sites and relative reactivity towards electrophilic and nucleophilic attack, and in the studies of biological recognition and hydrogen bonding interactions [47-49]. The 3D MEP of the title compound was calculated from optimized molecular structure by using B3LYP/6–311G (d,p) level and also shown in Fig. 11. The color scheme for the MEP surface is as follows: red for electron rich, partially negative charge; blue for electron deficient, partially positive charge; light blue for slightly electron deficient region; yellow for slightly electron rich region; green for neutral (zero potential); respectively. According to our results, the negative region (red) is located mainly over the O atomic sites, which are caused by the contribution of lone-pair electrons of the oxygen atom. The positive potential sites (blue) are located around the hydrogen and carbon atoms. A portion of the molecule that has a negative electrostatic potential will be susceptible to electrophilic attack; the more negative is the better. It is not as straightforward to use electrostatic potentials to predict nucleophilic attack [50]. Hence, the negative region (red) and positive region (blue) indicate electrophilic and nucleophilic attack symptoms. Also, a negative electrostatic potential region is observed around the $O_9$ atom.

The corresponding Mulliken's plot with B3LYP/6-311G (d,p) method is shown in Fig. 11. It is noted from Fig. 11 that strong negative and positive partial charges on the skeletal atoms (especially $O_9$, $O_{10}$, $C_1$, $C_2$, $C_3$, $C_4$, $H_5$, $H_6$, $H_7$, $H_8$) for the selected compounds increase with increasing Hammett constant of substituent groups [51, 52]. These distributions of partial charges on the skeletal atoms show that the electrostatic repulsion or attraction between atoms can contribute significantly to the intra- and intermolecular interaction.

### *NonLinear Optical (NLO) Analysis*

P-nitroaniline (PNA) is one of the prototypical molecules that are used in the study of the NLO properties of molecular systems. It is used frequently as a threshold value for comparative purposes and continues to be a recognized prototype of organic NLO chromophores. Its hyperpolarizability was studied both experimentally and theoretically in various solvents and at different frequencies [53–56]. Thus, we selected PNA as a reference molecule in this study, because there were no experimental values for 1,4-dioxane in the literature.

***Table 9: The ionization potential (I/eV), electron affinity (A/eV), chemical hardness (η/eV), softness (S/eV$^{-1}$), chemical potential (μ) and electronegativity (χ/eV), of 1,4-Dioxane using B3LYP/6-311G (d,P).***

| Compounds | I (eV) | A(eV) | X(eV) | (eV)μ | η (eV) | S(eV$^{-1}$) |
|---|---|---|---|---|---|---|
| 1,4-Dioxane | 5.225 | 0.278 | 2.751 | -2.751 | 2.473 | 0.202 |

***Table 10: Total static dipole moment (μ), the mean polarizability (<α>), the anisotropy of the polarizability (Δα), and the mean first-order hyperpolarizability (<β>) for 1,4-Dioxane using B3LYP/6-311G (d,P).***

| Property | PNA | B3LYP/6-311G(d,P) 1,4-Dioxane |
|---|---|---|
| $\mu_x$ | | 0.0000 Debye |
| $\mu_y$ | | 0.0000 Debye |
| $\mu_z$ | | 0.0000 Debye |
| μ | 2.44 Debye [a] | 0.0000 Debye |
| $\alpha_{XX}$ | | -36.4485 a.u. |
| $\alpha_{XY}$ | | -0.0001 a.u. |
| $\alpha_{YY}$ | | -26.3994 a.u. |
| $\alpha_{ZZ}$ | | -36.8630 a.u. |
| $\alpha_{YZ}$ | | 0.0003 a.u. |
| $\alpha_{XZ}$ | | 0.0000 a.u. |
| <α> | $22 \times 10^{-24}$ cm$^3$ [b] | $3.62 \times 10^{-24}$ esu |
| Δα | | $8.68 \times 10^{-24}$ esu |
| βxxx | | 0.000 a.u. |
| βxxy | | 0.000 a.u. |
| βxyy | | 0.000 a.u. |
| βyyy | | 0.000 a.u. |
| βxxz | | 0.000 a.u. |
| βxyz | | 0.000 a.u. |
| βyyz | | 0.000 a.u. |
| βxzz | | 0.000 a.u. |
| βyzz | | 0.000 a.u. |
| βzzz | | 0.000 a.u. |
| <β> | $15.5 \times 10^{-30}$ esu [c] | 0.000 esu |

a, b, c) PNA results are taken from references [60-62].

Polarizabilities and hyperpolarizabilities characterize the response of a system in an applied electric field [57]. They determine not only the strength of molecular interactions as well as the cross-sections of different scattering and collision processes, but also the non-linear optical (NLO) properties of the system [58, 59] In order to investigate the relationships among photocurrent generation, molecular structures and NLO, the polarizabilities and hyperpolarizabilities of title compound were calculated using B3LYP method, 6-311G (d,p) basis set, based on the finite-field approach. The mean first order hyperpolarizability ⟨$\beta$⟩, total static dipole moment (μ), the mean polarizability (<α>), and the anisotropy of the polarizability (Δα), of 1,4-dioxane are presented in Table 10. The calculated value of the dipole moment was found to be 0.00 D at B3LYP/6-311G (d,p).

***Table 11: Theoretical UV spectra of 1,4-Dioxane, calculated at TD-B3LYP/6–311G (d, p).***

| TD-Theoretical | | | | | | | | | | | | |
|---|---|---|---|---|---|---|---|---|---|---|---|---|
| Gas phase | | | | | water | | | | ethanol | | | |
| state | Configuration | Coefficient | f | λ, nm | Config uration | Coefficient | f | λ, nm | Configuration | Coefficient | f | λ, nm |
| I | 21-> 23 22->26 | 0.55<br>0.42 | 0.51 | 148 | 21-> 23 22-> 25 | 0.55<br>0.42 | 0.60 | 21->23 22 ->25 | 151 | 0.61 | 0.55<br>0.42 | 151 |
| II | 19 ->23 | 0.70 | 0.14 | 131 | 19->23 | 0.70 | 0.18 | 19 ->23 | 131 | 0.18 | 0.70 | 131 |
| III | 21->25 | 0.70 | 0.02 | 140 | 21->26 | 0.70 | 0.02 | 21 ->26 | 136 | 0.02 | 0.70 | 136 |
| IV | 18-> 23 | 0.70 | 0.01 | 129 | 18->23 | 0.70 | 0.01 | 18 ->23 | 131 | 0.01 | 0.70 | 130 |

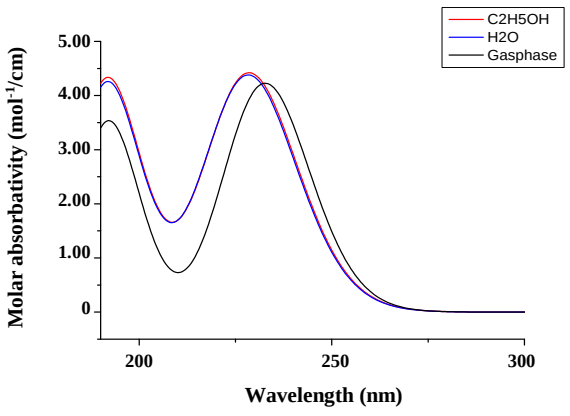


***Fig. 12: Electronic absorption spectra of 1,4-Dioxane.***

The calculated mean polarizability (<α>) is 3.62x10$^{-24}$esu, i.e. two times smaller than PNA molecule. In addition, the calculated mean first order hyperpolarizability⟨$\beta$⟩, of the title molecule is 0.00 esu i.e. smaller than PNA molecule [60-62]. These results indicate the linearity of the title molecule and show that it cannot be used as NLO materials.

***Electronic absorption spectra of dioxane***

The theoretical electronic spectra of 1,4-dioxane in 10% ethanol/90% water solvent mixture and the assignment of the spectra are given in Fig. 12 and Table 11. The charge density maps of the occupied and vacant MO's considered in the transitions are presented in Figs. (13 and 14). The spectrum in ethanol/water is composed of four bands centered at 151 nm, 131 nm, 136 nm, and 130 nm. All bands are assigned to (π-π*) transitions as reflected in their intensities (0-500). The excited configurations considered in 1,4-dioxane are those which result from an electron excitation of five highest occupied molecular orbitals $\varphi_{18}^{-1}\varphi_{22}$ and the lowest five vacant molecular orbitals $\varphi_{23}^{-1}\varphi_{27}$.

The first $(\pi\text{-}\pi^*)^1$ state is centered at 151 nm in ethanol and water and in the gas phase at 148 nm this band

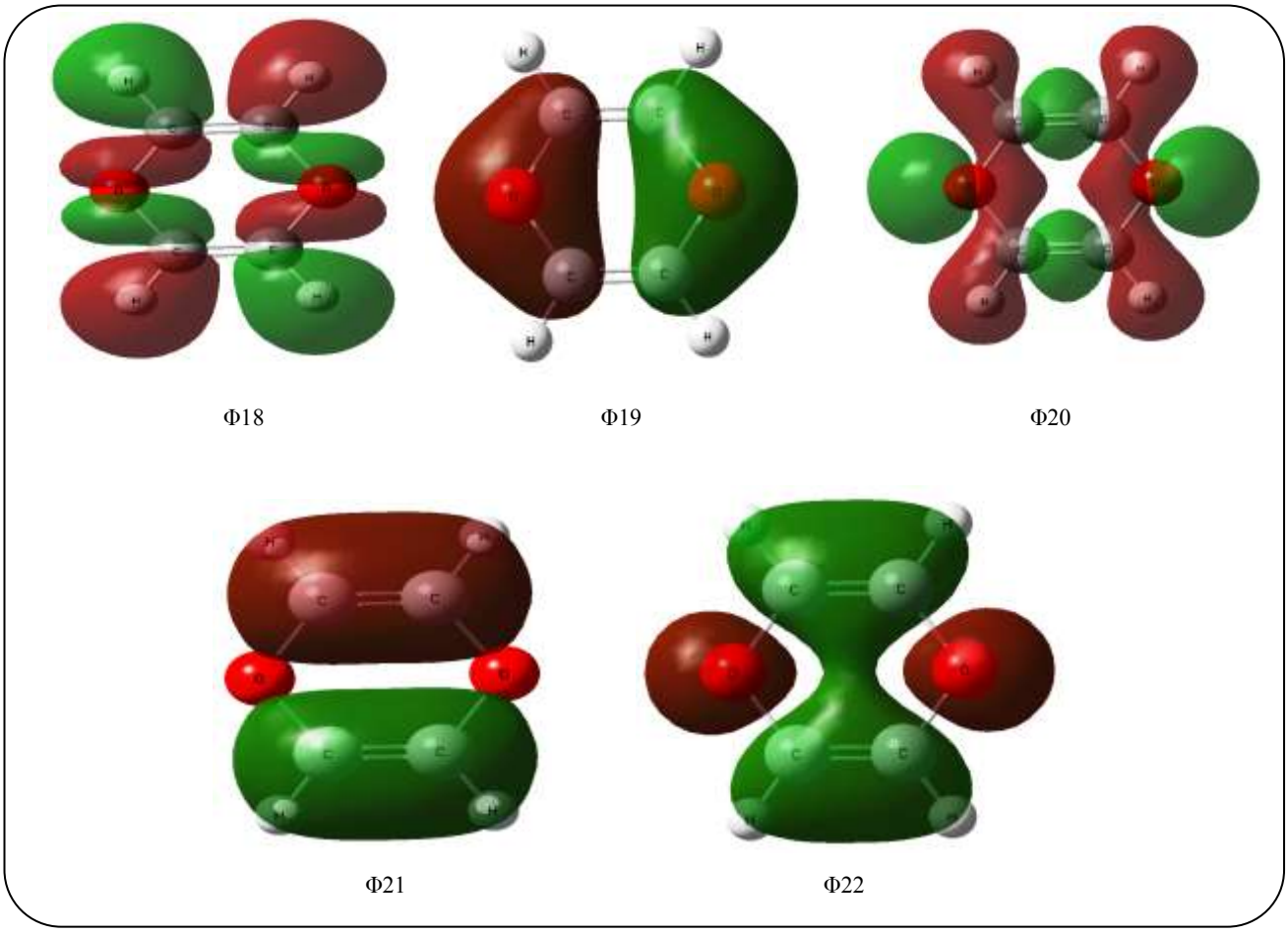


***Fig. 13: The charge density maps of the occupied of 1,4-Dioxane.***

is composed of a mixture of two configurations, (c.f. Table 11) and assigned as CT, and delocalized configurations may be expected. The second $(\pi\text{-}\pi^*)^1$ state is centered at 131 nm in ethanol and water and in the gas phase at 131 nm. This state is composed of one configuration, namely, $\varphi_{19}^{-1}\varphi_{23}$, that is, CT character may be expected (Figs. 13 and 14). The third $(\pi\text{-}\pi^*)^1$ state is centered in ethanol/water at 136 nm and in the gas phase at 140 nm. This band is composed of one configuration, (Table 11) and assigned as CT character. The fourth $(\pi, \pi^*)^1$ state computed at 130 nm in ethanol/water, and in the gas phase at 129 nm. This state is composed of one configuration, which is also assigned as a charge transfer band (CT) (Figs. 13 and 14).

## CONCLUSIONS

The molecular geometry of 1,4-dioxane in the ground state has been calculated by using density function theory (DFT-B3LYP/6-311G (d,p). The optimized structure of the molecule is planar as indicated from the dihedral angles. The HOMO-LUMO energy gap helped in analyzing the chemical reactivity, hardness, softness, chemical potential, and electronegativity. We studied the Mullikan and natural charge distribution of 1,4-dioxane and the study determined the electronic charge distribution in 1,4-dioxane. The calculated dipole moment and the first order hyperpolarizability results indicate that 1,4-dioxane has a reasonable bad linear optical behavior. The NBO analysis indicated the intermolecular charge transfer between the bonding and anti-bonding orbitals. MEP confirmed the different negative and positive potential sites of the molecule in accordance with the total electron density surface. All bands in the UV spectra can be assigned to $(\pi\text{-}\pi^*)$ transitions as reflected from their intensities. According to the high activity in physical parameters of 1,4-dioxane, the $E_{HOMO}$, $E_{LUMO}$, $E_{gap}$ and dipole moment ($\mu$) were applied to the interaction with nano-$CuSO_4$ solutions in 10% ethanol–water form 1:1 and 1:2 M/L complexes.

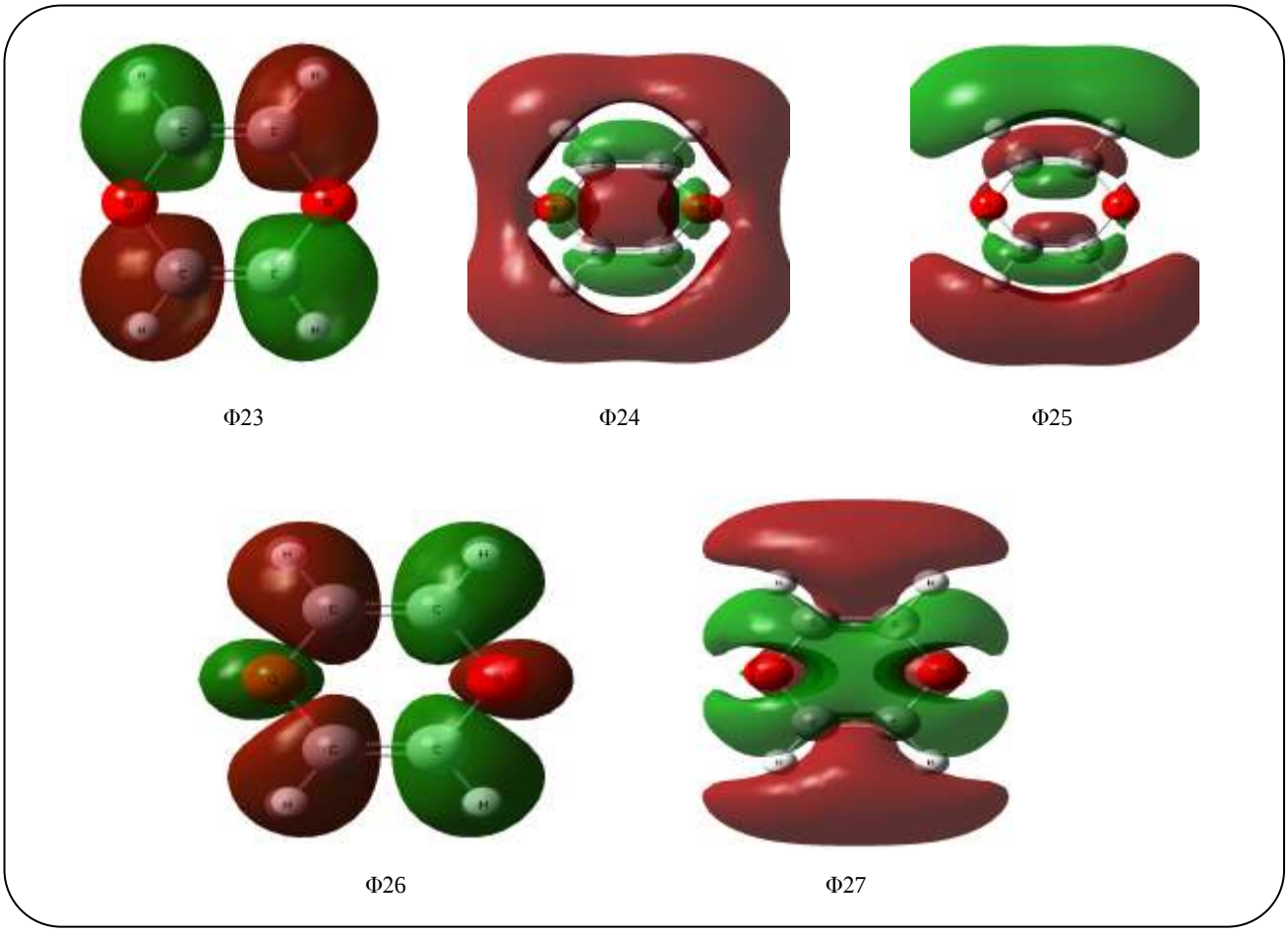


***Fig. 14: The charge density maps of the unoccupied of 1,4-Dioxane.***

Increasing the thermodynamic parameters, Gibbs free energies, enthalpies and entropies of solvation increasing the temperature indicate more interactions.

*Received : Nov.. 24, 2017 ; Accepted : April 23, 2018*

**REFERENCES**

[1] Eusebio Juarist,, Giselle A. Rosquete-Pina, Maribel Vázquez-Hernández, Antonio J. Mota, Salt Effects on the Conformational Behavior of 5-substituted 1,3-dioxanes, *Pure Appl. Chem.*, **75**: 589-620 (2003).

[2] Bushweller, C. H., "Stereochemistry of Cyclohexane and Substituted Cyclohexanes. Substituted A Values in Conformational Behavior of Six-Membered Ring Analysis, Dynamics and Stereoelectronic Effects", Juaristi, E., (Ed.); VHC/Wiley: New York, Chapter 2 (1995).

[3] Wiberg K.B., Hammer J.D., Castejon H., Bailey W.F., DeLeon E.L., Jarret R.M., Conformational Studies in the Cyclohexane Series. 1. Experimental and Computational Investigation of Methyl, Ethyl, Isopropyl, and Tert-butylcyclohexanes, *J. Org Chem.*, **64**(6): 2085-2095 (1999).

[4] Salzner U., Schleyer P.V.R., Ab Initio Examination of Anomeric Effects in Tetrahydropyrans, 1,3-Dioxanes, and Glucose, *J. Org. Chem.*, **59**: 2138-2148 (1994).

[5] Dabbagh H.A., Modarresi-Alam A.R., Tadjarodi A., Taeb A., Experimental Demonstration of Anomeric Effect and structure: X-Ray Conformational and Configurational Analysis of *N*-2-(1,4-dioxane)-*N'*-(*p*-methylbenzenesulfonyl)-*O*-(*p*-methylphenoxy) Isourea, *Tetrahedron*, **58**: 2621-2632 (2002).

[6] Arnaud-Neu F., Delgado R., Chaves S., Critical Evaluation of Stability Constants and Thermodynamic Functions of Metal Complexes of Crown Ethers, *Pure. Appl. Chem*., **75**: 71-102 (2003).

[7] Wong P.S.H., Antonio B.J., Dearden D.V., Gas-Phase Studies of Valinomycin-Alkali Metal Cation Complexes: Attachment Rates and Cation Affinities., *J. Am. Soc. Mass Spectrosc.*, **5**: 632 – 637 (1994).

[8] Andreas T., Tsatsas, Robert W., Stearns, William, Risen M., Nature of Alkali Metal Ion Interactions with Cyclic polyfunctional Molecules. I. Vibrations of Alkali Ions Encaged by Crown Ethers in Solution., *J. Am. Chem. Soc.*, **94**: 5247- 5253 (1972).

[9] Popov A.I., Lehn J.M., In: Melson G.A. (Ed.), "Coordination Chemistry of Macrocyclic Compounds", Plenum Press, New York, (1979).

[10] Mandal K., Kar T., Nandi P.K., Bhattacharyya S.P., Theoretical Study of the Nonlinear Polarizabilities in $H_2N$ and $NO_2$ Substituted Chromophores Containing Two Hetero Aromatic Rings, *Chem. Phys. Letts.*, **376**: 116-124 (2003).

[11] Nandi P.K., Mandal K., Kar T., Effect of Structural Changes in Sesquifulvalene on the Intramolecular Charge Transfer and Nonlinear Polarizations-A Theoretical Study, *Chem., Phys. Letts.*, **381**: 230-238 (2003).

[12] Prasad P.N., Williams D.J., "Introduction to Nonlinear Optical Effects in Molecules and Polymers", John Wiley & Sons, Inc., New York, NY, USA (1991).

[13] Meyers F., Marder S.R., Pierce B.M., Brédas J.L., Electric Field Modulated Nonlinear Optical Properties of Donor-Acceptor Polyenes: Sum-Over-States Investigation of the Relationship between Molecular Polarizabilities (.alpha., .beta., and .gamma.) and Bond Length Alternation, *J. Am. Chem. Soc.*, **116**: 10703-10714 (1994).

[14] Foster J.P., Weinhold F., Natural Hybrid Orbitals, *J. Am. Chem. Soc.*, **102**: 7211-7218 (1980).

[15] Reed A.E., Curtiss L.A., Weinhold F., Intermolecular Interactions from a Natural Bond Orbital, Donor-Acceptor Viewpoint, *Chem. Rev.*, **88**: 899- 926 (1988).

[16] Holleman A.F., Wiberg E., "Inorganic Chemistry", ISBN 0-12-352651-5, San Diego: Academe. Press. (2001).

[17] David A., "Wright and Pamela Welbourn Environmental Toxicology", Cambridge University Press, UK (2002).

[18] Abou Elleef. El Sayed M., Gomaa. Esam A., Thermodynamics of solvation for Nano Zinc Oxide in 2 M $NH_4Cl$ + Mixed DMF - $H_2O$ Solvent at Different Temperature, *International Journal of Engineering and Innovative Technology*, **2**: 121-126 (2013).

[19] Gomaa E.A., Ibrahim K.M., Hassan N.M., Thermodynamics of Complex Formation (conductometrically) between Cu(II) Ion and 4-phenyl-1-diacetyl monoxime-3-Thiosemicarbazone (BMPTS) in Ethanol at Different Temperatures, Research and Reviews, *Journal of Chemistry*, **3**: 47-55 (2014).

[20] (a) Becke A., Density functional Thermochemistry. II. The Role of Exact Exchange, *Chem. Phys.*, **98**: 5648-5652 (1993).
(b) Becke A., Density Functional Thermochemistry. III. The Role of Exact Exchange, *Chem. Phys.*, **98**: 1372-1376 (1993).

[21] Lee C., Yang W., Parr R.G., Development of the Colle-Salvetti Correlation-Energy Formula into a Functional of the Electron Density, *Phys. Rev. B Condens. Matter.*, **15**: 785-789 (1988).

[22] Stefanov B, Liu B.G., Liashenko A., Piskorz P., Komaromi I., Martin R.L., Fox D.J., Keith T., Al-Laham M.A., Peng C.Y., Nanayakkara A., Challacombe M., Gill P.M. W., Johnson B., Chen W., Wong M.W., Gonzalez C., Pople J.A., Gaussian, Inc., Pittsburgh PA (2003).

[23] Kuz'min I.V., Solkan V.N., Zhidomirov G.M., Kanzanski V.B., Modling of the Mechanism of One Electron Transfer from the Perylene Molecule to Oxygen Molecule $^3O_2$ in HF Medium., *SN Applied Sciences*, **52**: 192-203 (2011).

[24] Dennington, Keith R., Millam T., Semichem J., GaussView, Version 5 Inc., Shawnee Mission KS (2009).

[25] Avci D., Second and Third-Order Nonlinear Optical Properties and Molecular Parameters of Azo Chromophores: Semiempirical Analysis, *Spectrochimica Acta A.*, **82**: 37- 43 (2011).

[26] Avci D., Başoğlu A., Atalay Y., NLO and NBO Analysis of Sarcosine Maleic Acid by Using HF and B3LYP Calculations, *Struct. Chem.*, **21**: 213-219 (2010).

[27] Avci D., Cömert H., Atalay Y., Ab initio Hartree-Fock Calculations on Linear and Second-Order Nonlinear Optical Properties of New Acridine-Benzothiazolylamine Chromophores, *J. Mol. Modeling.*, **14**: 161- 171 (2008).

[28] Pearson R.G., Absolute Electronegativity and Hardness Correlated with Molecular Orbital Theory, *Proc. Nat. Acad. Sci*., **83**: 8440 – 8441 (1986).

[29] Chandra A.K., Uchimara T., NLO and NBO Analysis of Sarcosine-Maleic Acid by Using HF and B3LYP Calculations, *J. Phy. Chem. A*, **105**: 3578 – 3582 (2001).

[30] Chocholoušová J., Špirko V., Hobza P., First Local Minimum of the Formic Acid Dimer Exhibits Simultaneously Red-Shifted O–H···O and Improper Blue-Shifted C–H…O Hydrogen Bonds, *Phys. Chem.*, **6**: 37- 41 (2004).

[31] Szafran M., Komasa A., Bartoszak-Adamska E., Crystal and Molecular Structure of 4-Carboxypiperidinium Chloride (4-Piperidinecarboxylic Acid Hydrochloride), *J. Mol. Struct.*, **827**: 101-107 (2007).

[32] Ives D.J.G., "Chemical Thermodynamics", University Chemistry, Maconald Technical and Scientific (1971).

[33] Dickenson R.E., Geis I., "Benjamin Chemistry", W.A., Matter, and the Universe, Inc., USA (1976).

[34] Oswal S.L., Desai J.S., Ijardar S.P., Jain D.M., Studies of Partial Molar Volumes of Alkylamine in Non-Electrolyte Solvents II. Alkyl Amines in Chloroalkanes at 303.15 and 313.15 K, *J. Mol. Liquids*, **144**: 108-114 (2009).

[35] Zhang D.E., Zhang X.J., Ni X.M., Zheng H.G., Yang D.D., Synthesis and Characterization of $NiFe_2O_4$ Magnetic Nanorods via a PEG-Assisted Route, *J. Magn. Mater.*, **292**: 79-82 (2005).

[36] Xia B.Y., Yang P.D., Sun Y.G., One-Dimensional Nanostructures: Synthesis, Characterization, and Applications, *Adv. Mater.*, **15**: 353-356 (2003).

[37] Duan X., Huang Y., Cui Y., Wang J., Lieber CM., Indium Phosphide Nanowires as Building Blocks for Nanoscale Electronic and Optoelectronic Devices, *Nature* 66-69 (2001).

[38] Hamed Mohamed N.H., Gomaa Esam A., Sanad Sameh G., Thermodynamics of Solvation for Nano Zinc Carbonate in Mixed DMF–$H_2O$ Solvents at Different Temperatures, *International Journal of Engineering and Innovative Technology (IJEIT)*, 4: 203 – 207 (2014).

[39] Liu W.J., He W.D., Zhang Z.C., Nanogenerators-from Scientific Discovery to Future Applications, *J. Cryst. Growth.*, **290**: 592-598 (2006).

[40] Marcus Yizahak, Solubility and Solvation in Mixed Solvent Systems, *Pure and Applied Chem.*, **62**: 2069 – 2076 (1990).

[41] Chen L., Shen L., Xie A., Zhu J., Wu Z., Yang L., Discovery of Diamond in Eclogite from the Chinese Continental Scientific Drilling Project Main Hole (CCSD-MH) in the Sulu UHPM Belt, *Cryst. Res. Technol.*, **42**: 886- 891 (2007). [in Chinese]

[42] Yurii A., Simonov, A. Alexandr, Dvorkin, Marina, S. Fonari, Tadeush, I. Malinowski, Elzbieta Luboch, Andrzej Cygan, Jan F. Biernat, V. Edward, Ganin, Popkov., Investigation of Structural, Thermal and Magnetic Behaviors of Pristine Barium Carbonate Nanoparticles Synthesized by Chemical Co-Precipitation Method, *J. Inclusion Phenomena and Molecular Recognition in Chemistry*, **15**: 79-85 (1993).

[43] Snehalatha M., Ravikumar C., Hubert Joe I., Sekar N., Jayakumar V.S., Vibrational Spectra and Scaled Quantum Chemical Studies of the Structure of Martius Yellow Sodium Saltmonohydrate, *Spectrochim. Acta A*, **40**: 1121-1126 (2009).

[44] James C., Amal A., Raj, Reghunathan R., Joe I.H., Jayakumar V.S., Structural Conformation and Vibrational Spectroscopic Studies of 2, 6-bis (p-N, N-dimethyl benzylidene) Cyclohexanone using Density Functional Theory, *J. Raman Spectrosc*, **37**: 1381- 1392 (2006).

[45] Liu J., Chen Z., Yuan S., Zhejiang J., Study on the Prediction of Visible Absorption Maxima of Azobenzene Compounds, *Univ. Sci. B*, **6**: 584 – 589 (2005).

[46] Rubarani P., Gangadharan S., Sampath Krishnan, Natural Bond Orbital (NBO)Population Analysis of 1-Azanapthalene-8-ol, *Acta Physica Polonica A*, **125**: 18-22 (2014).

[47] Scrocco E., Tomasi J., Interpretation by Means of Electrostatic Molecular Potentials, *Advances in Quantum Chemistry*, **11**: 115-120 (1979).

[48] Luque F.J., López J.M., Orozco M., Electrostatic Interactions of a Solute with a Continuum. A Direct Utilization of ab initio Molecular Potentials for the Prevision of Solvent Effects, *Theoret. Chem. Accounts*, **103**: 343-345 (2000).

[49] Okulik N., Jubert A.H., Theoretical Analysis of the Reactive Sites of Non-Steroidal Anti-Inflammatory Drugs, *Int. Elect. J. Mol. Des.*, **4**: 17-30 (2005).

[50] Politzer P., Murray J.S., The Fundamental Nature and Role of the Electrostatic Potential in Atoms and Molecules, *Theor. Chem. Acc.*, **108**: 134-142 (2002).

[51] Sajan D., Joseph L., Vijayan N., Karabacak M., Natural bond Orbital Analysis, Electronic Structure, Non-Linear Properties and Vibrational Spectral Analysis of l-Histidinium Bromide Monohydrate: A Density Functional Theory, *Spectrochim. Acta A*, **81**: 85-98 (2011).

[52] Hansch C., Leo A., Taft R.W., A Survey of Hammett Substituent Constants and Resonance and Field Parameters, *Chem. Rev.*, **91**: 165-195 (1991).

[53] Jensen L., Van Duijnen P.T., The First Hyperpolarizability of p-Nitroaniline in 1,4-Dioxane: A Quantum Mechanical/Molecular Mechanics Study, *J. Chem. Phys.*, **123** Article ID 074307 (2005).

[54] Sałek P., Vahtras O., Helgaker T., Ågren H., Density-Functional Theory of Linear and Nonlinear Time-Dependent Properties Molecular, *J. Chem. Phys.*, **117**: 9630-9635 (2002).

[55] Stähelin M., Burland D.M., Rice J. E., Sign Change of Hyperpolarizabilities of Solvated Water, *Chem. Phys. Lett.*, **191**: 245-250 (1992).

[56] Huyskens F.L., Huyskens P.L., Persoons A.P., Solvent Dependence of the First Hyperpolarizability of *p*-nitroanilines: Differences between Nonspecific Dipole–Dipole Interactions and Solute–Solvent H-Bonds, *J. Chem. Phys.*, **108**: 8161-8168 (1998).

[57] Zhang C.R., Chen H.S., Wang G.H., Geometry, Electronic Structure, and Related Properties of Dye Sensitizer: 3,4-bis[1-(carboxymethyl)-3-indolyl]-1H-pyrrole-2,5-dione, *Chem. Res. Chin. U*, **20**: 640-646 (2004).

[58] Sun Y., Chen X., Sun L., Guo X., Lu W., A Monolayer Organic Light-Emitting Diode Using an Organic Dye Salt, *Chem. Phys. Lett.*, **83**: 1020-1022 (2003).

[59] Christiansen O., Gauss J., Stanton J.F., Non-Linear Optical Properties of Matter, *Chem. Phys. Lett.*, **305**: 51-99 (1999).

[60] Cheng L.T., Tam W., Stevenson S.H., Meredith G.R., Rikken G., Marder S.R., Experimental Investigations of Organic Molecular Nonlinear Optical Polarizabilities. 1. Methods and Results on Benzene and Stilbene Derivatives, *J. Phys. Chem.*, **95**: 10631-10643 (1991).

[61] Karna S.P., Prasad P.N., Dupuis M., Nonlinear Optical Properties of Novel Thiophene Derivatives: Experimental and ab initio Time-Dependent Coupled Perturbed Hartree–Fock Studies, *J. Chem. Phys.*, **94**: 1171-1179 (1991).

[62] Kaatz P., Donley E.A., Shelton D.P., A Comparison of Molecular Hyperpolarizabilities from Gas and Liquid Phase Measurements, *J. Chem. Phys.*, **108**: 849-855 (1998).